Available online at www.sciencedirect.com
ScienceDirect
Journal of Power Sources 163 (2007) 900–906
JOURNAL OF POWER SOURCES
www.elsevier.com/locate/jpowsour

Fracture strength of micro-tubular solid oxide fuel cell anode in redox cycling experiments

Jakub Pusz [a,*], Alevtina Smirnova [a], Alidad Mohammadi [a], Nigel M. Sammes [a,b]

[a] *Department of Chemical, Materials, and Biomolecular Engineering, University of Connecticut, 44 Weaver Road, Storrs, CT 06269, USA*
[b] *Department of Mechanical Engineering, University of Connecticut, 44 Weaver Road, Storrs, CT 06269, USA*

Received 8 August 2006; received in revised form 27 September 2006; accepted 29 September 2006
Available online 17 November 2006

Abstract

The maximum fracture strength of Ni/8YSZ anodes exposed to several redox cycles is compared. The anodes were fabricated using fine and coarse particle size powders. Fine-structured powders show a 77% increase in mechanical strength after exposure to three redox cycles. The coarse-structured material did not produce similar results and redox cycling resulted in gradual decrease in the mechanical stability of the supports.

The impact of redox cycling on the microstructure was evaluated using SEM. Fine-structured anodes tend to agglomerate leading to decreased porosity. Coarse anodes did not show any significant changes in microstructure while exposed to redox cycling.

The electrochemical performance evaluated under load conditions, and after the first redox cycle, indicates a 40% improvement for the cell fabricated using a fine-structured anode powder. The increase in performance is believed to be due to better adhesion between the anode material and the Ni current collector. The cell fabricated using a coarse-structured anode powder did not recover after the redox cycle.

Keywords: SOFC; Redox; Anode; Strength; Morphology; Particle size

1. Introduction

Solid oxide fuel cells (SOFC) fabricated using a standard nickel–cermet anode, presents good catalytic activity towards the oxidation of hydrogen and hydrocarbon fuels [1–7]. In order to improve long-term stability of the anode, nickel is typically mixed with yttria stabilized zirconia. A mixture of coarse and fine particles are traditionally used whereby coarse particles are usually 25 μm or larger [8], and are responsible for matching the thermal expansion coefficient of the YSZ electrolyte layer. The fine particles are approximately 0.5 μm in size and prevent nickel from agglomeration and co-sintering. Such a composition of anode substrate prevents delamination and cracking of the electrolyte layer due to the thermal expansion mismatch as well as keeping the desired anode porosity. This approach improves long-term mechanical stability of Ni/YSZ-based materials operated under a reducing environment. Exposure of nickel–cermet anode to reoxidation, however, results in change of the physical and mechanical properties that potentially leads to failure of the cell.

Work has shown that redox cycling results in volumetric changes of the cermet anode [9]. The studies show that the kinetics of Ni oxidation is dependent upon powder processing procedures, especially surface preparation, grain/particle size, and impurity levels [9–12]. The fine-structured anodes experience no change in volume upon reduction; yet, a 2–2.5% increase in volume occurs during reoxidation [9]. Such an expansion could potentially result in an increase of the internal stresses of the nickel crystal structure which could affect the integrity of the cell. Additionally, volumetric changes over the electrode–electrolyte layer are likely to result in delamination of the electrolyte and micro-crack formation [9].

The change in mechanical and microstructural properties of the anode is expected to affect both the mechanical strength and the electrochemical performance of the cell. However, the results of the studies might be highly dependent upon the powder processing technologies and cell fabrication techniques.

This paper describes the response of the anode supports, fabricated from coarse and fine materials, to redox cycling.

* Corresponding author. Tel.: +1 860 486 5407; fax: +1 860 486 8378.
E-mail address: jpusz@engr.uconn.edu (J. Pusz).

0378-7753/$ – see front matter © 2006 Elsevier B.V. All rights reserved.
doi:10.1016/j.jpowsour.2006.09.074

2. Experimental

2.1. Mechanical testing

Tubular anodes, of final dimensions 5.63 mm i.d. and 7.31 mm o.d., were fabricated using two different commercially available anode powders; a fine particle size powder and a coarse particle size.

The fine particle size powder was a premixed 50/50 by volume ratio of black nickel oxide nanopowder (NiO) (99.9%, average particle size 20–50 nm) and 8 mol% yttria stabilized zirconia nanopowder (8YSZ) (99.9%, average particle size 40–60 nm). The powder is commercially available as Nanox 28ZY8-1C by Inframat Advanced Materials.

The coarse particle size powder was a premixed 50/50 by volume ratio (after reduction) nickel oxide (average particle size 0.92 μm) and 8YSZ (NexTech Materials).

Both of the anode substrates were separately prepared in the same way. The anode powders were mixed with Methocel A4M polymer binder (5 wt%) and Vulcan XC605 carbon poreformer by Cabot (20 vol% of NiO/8YSZ powder). The powders were mixed with 12 wt% of de-ionized water in a SK-6 Jaygo mechanical mixer.

The extruded anodes were fired at 1500 °C according to the following scheme:

Stage 1: Heated to 500 °C at 1 °C min^{-1} ramp rate.
Stage 2: Dwell for 2 h in order to burn out carbon poreformer and binder.
Stage 3: Heated to 1500 °C at 1 °C min^{-1} ramp rate.
Stage 4: Dwell for 2 h in order to sinter the anode.
Stage 5: Cooled down at 5 °C min^{-1} ramp rate.

The following procedure of sample preparation was performed for both, fine and coarse-structured anode powders.

The tubes were cut into 70 rings, each 5 mm long, and the edges were polished using a 1200 grit size SiC abrasive. A longitudinal cut was made using a diamond blade to form a notch 1 mm wide, resulting in a C-ring structure (Fig. 1).

Sixty rings were reduced overnight in a quartz tube continuously purged with hydrogen at 0.08 L min^{-1} flow rate. The tube was mounted inside a small tubular furnace maintained at 800 °C. After the furnace was cooled down, 10 rings were removed while the remaining rings were subjected to redox cycling.

The redox cycling was performed at 800 °C in five steps according to the scheme: $H_2 \rightarrow N_2 \rightarrow Air \rightarrow N_2 \rightarrow H_2$. Initially, the reduced C-rings were heated to 800 °C, at 6 °C min^{-1} ramp rate, with hydrogen continuously purged at 0.08 L min^{-1}. After the temperature was reached, the quartz tube was purged with nitrogen at 0.1 L min^{-1} for 30 min. Following this step, air was provided at a constant flow rate of 1.0 L min^{-1} for 1 h. The system was then purged with nitrogen for 30 min at 0.1 L min^{-1} flow rate. In the final step, the C-rings were re-reduced with hydrogen at 0.08 L min^{-1} flow rate for 1 h and the furnace was cooled down at a constant rate of 6 °C min^{-1} with hydrogen

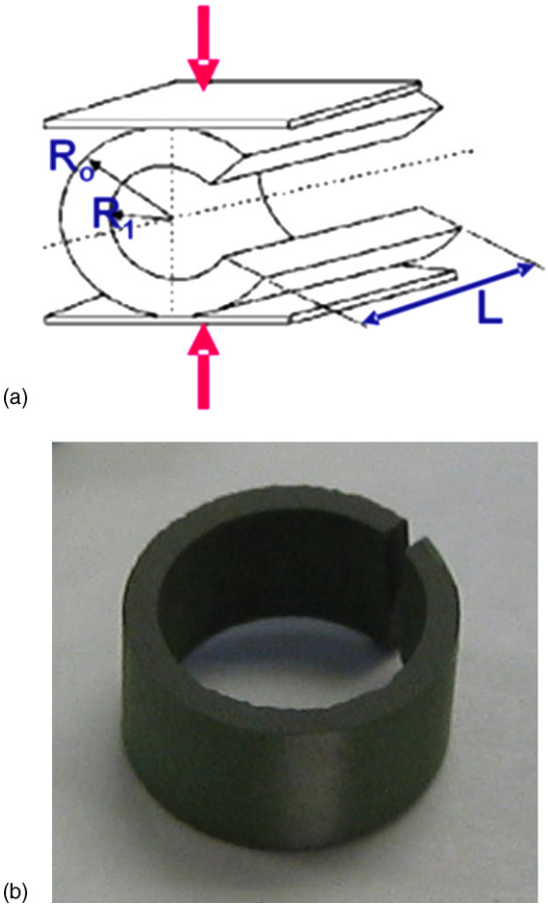

Fig. 1. (a) C-ring configuration for strength measurement of anode tubes; (b) slice of anode-supported tube for fracture strength testing.

continuously purged through the system. After the furnace was cooled down, 10 samples were removed and the remaining samples were re-subjected to redox cycles according to the same scheme. In total, five redox cycles were performed.

Mechanical testing of the reduced anode tubes was performed using an Instron 5866 model. The strength of the C-rings was determined according to the standard test for ultimate strength of advanced ceramics with diametrally compressed C-ring specimens at ambient pressure (ASTM C 1323-96).

The maximum fracture strength was calculated according to the equation:

$$\sigma_{max} = \frac{PR}{LtR_0}\left[\frac{R_0 - R_a}{R_a - R}\right] \quad (1)$$

$$R = \frac{R_0 - R_1}{\ln(R_0 - R_1)} \quad (2)$$

where R_0 is the outer radius of the C-ring; R_1 the inner radius of the C-ring; R_a the average of R_0 and r_i; L the length of the ring; t thickness of the wall; P is the fracture of the load applied to the C-ring.

Each sample from the cycle was measured and σ_{max} was calculated using Eqs. (1) and (2). The results were used to estimate the average value of σ_{max} and the respective standard deviation for each of the cycles.

In order to study any microstructural changes that occurred during redox cycling, SEM micrographs of the samples were taken before and after each redox cycle, using a JEOL JSM-5600LV Scanning Electron Microscope.

2.2. Electrochemical testing

The single cell was electrochemically tested in a small tubular Carbolite furnace. The cells were prepared using methods described in Ref. [13]. Nickel spring, and silver wire painted with silver paste (Alfa Aesar) were used for the anode and cathode current collectors respectively. The inlet of the cell was sealed to an alumina tube, which served as a mechanical support and a fuel line, using ceramic glue (Ceramabond 552). The seal was kept outside of the furnace to prevent any hydrogen leak that might reduce the lanthanum strontium manganite (LSM) cathode. Preheated air circulation on the cathode side of the cell was provided using a small air pump.

The cell was continuously purged with nitrogen and heated up to 800 °C with a ramp of 5 °C min^{-1}. After the temperature was reached, hydrogen was provided at 0.5 L min^{-1} flow rate and the cell was reduced overnight.

After a stable open circuit voltage (OCV) was reached the cell was operated at constant current condition of 0.75 A cm^{-2}. The cell was maintained under load conditions for 72 h in order to reach a stable performance; this stage was then followed by the redox cycle.

The redox cycle consisted of a series of steps. Initially, the cell was purged with nitrogen at 0.5 L min^{-1} for 15 min followed by oxidation with air at the flow rate of 1 L min^{-1} for 30 min. The system was again purged with nitrogen at 0.5 L min^{-1} flow rate for 15 min to remove the air. Finally, the cell was exposed to hydrogen flow at 1 L min^{-1}. After the OCV was restored, the cell was operated at constant current for 30 min. In total, the cell was exposed to two redox cycles.

3. Results and discussion

3.1. Mechanical testing

3.1.1. Fine-structured anode powder

The results of the mechanical testing after each redox cycle are plotted in Fig. 2. No significant increase in mechanical strength was observed between the non-reduced and reduced anode. However, the first redox cycle resulted in a 43% increase in the mechanical strength, compared to the reduced anode. The maximum strength of the rings, which was obtained after the third redox cycle, was 77% higher than the reduced anode. Further cycles resulted in a decrease of the fracture stress. However, the strength of the samples remained higher than the non-reoxidized anodes.

In order to verify the accuracy of data, the Weibull parameter was calculated for every cycle and is presented in Table 1. Even though the test of mechanical strength after the third redox cycle produced uniform data, a large spread of data points, accompa-

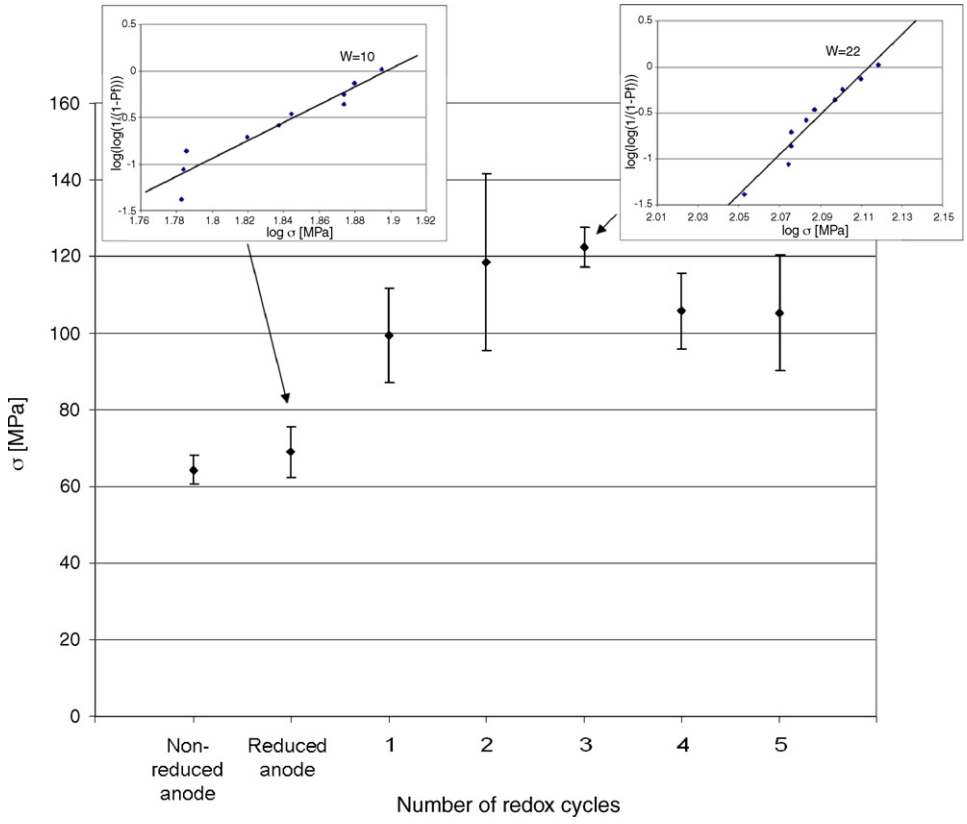

Fig. 2. Strength (σ) of the C-shaped uniaxially compressed fine-structured anode rings vs. number of redox cycles. Two Weibull plots, of reduced anode and anode after three redox cycles, represent the accuracy of obtained data. Accurate data is characterized by Weibull parameter "*W*" of 10 or larger.

Table 1
Average sigma, standard deviation and Weibull parameter of fine-structured anode rings for all cycles

Cycle	σ_{avg} (Mpa)	Standard deviation	Weibull parameter
Non-reduced anode	65.1	3.8	16
Reduced anode	69.0	6.7	10
First redox	98.6	12.5	8
Second redox	118.0	23.0	5
Third redox	122.4	5.5	22
Fourth redox	105.3	9.8	10
Fifth redox	105.3	15.8	6

nied by a value of the Weibull parameter lower than 10, was observed for the second redox cycle. The spread in data points suggest that major microstructural changes occurred after the second redox cycle.

The SEM micrographs showed a significant change in the anode microstructure (Fig. 3). The micrographs suggested that nickel particles agglomerated and sinter thus leading to decreased porosity. As a result of particles cohesion mechanical strength improved.

3.1.2. Coarse-structured anode powder

The comparison of the mechanical strength of fine and coarse-structured anode powders after redox cycling is presented in Fig. 4. The study showed that the response of the cell to exposure to redox cycling is different for anodes of coarse and fine morphology. While the fine-structured anode rings presented an increase in mechanical strength upon redox cycling, the anode rings that were characterized by coarse particle sizes showed a gradual decrease of the fracture strength after redox cycling. In general, coarse particle sized anodes presented much lower mechanical strength in each of the cycles.

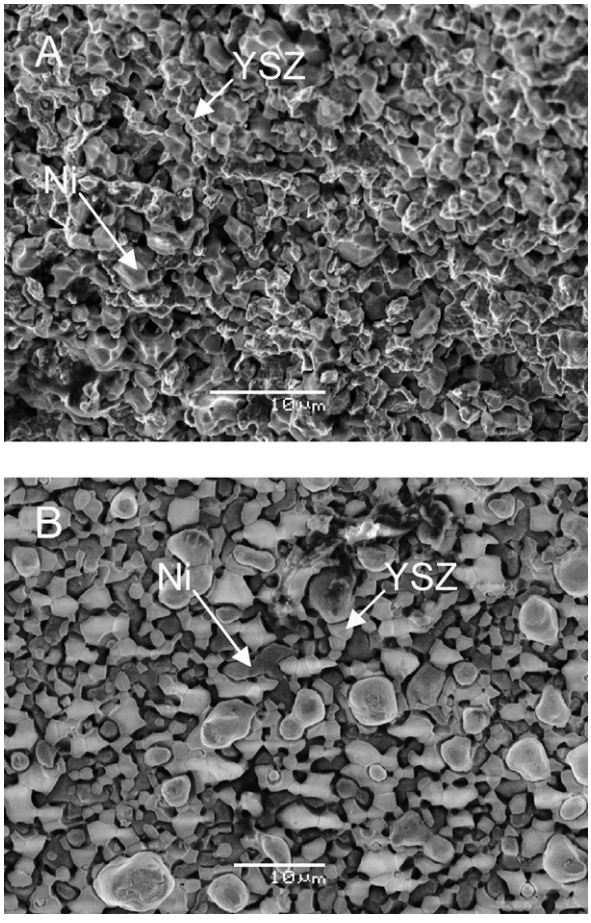

Fig. 3. SEM micrographs of the fine-structured Ni/8YSZ anodes (A) after reduction and (B) after the third redox cycle.

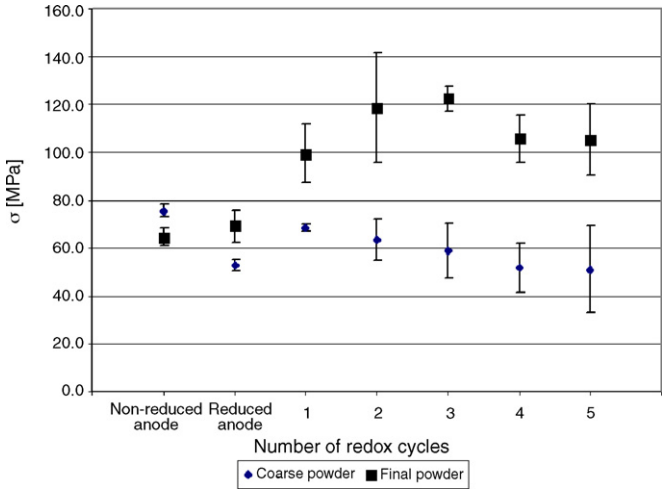

Fig. 4. Strength (σ) of the C-shaped uniaxially compressed anode rings vs. number of redox cycles. The samples were fabricated using two different powders, coarse and fine structured.

A comparison of values for every cycle of the average fracture strength, standard deviation and Weibull parameter, of coarse and fine-structured anodes, is presented in Table 2. Coarse-structured anode supports presented a low standard deviation of the data in the first cycles. This implies that the microstructural changes of the anode were uniform for all the samples. Further spread in data points represents a major mechanical degradation of the nickel crystal structure resulting in non-uniform maximum fracture strength.

Coarse-structured anodes do not expand significantly during reoxidation and the morphology does not seem to change significantly. However, fine-structured powders show large volumetric changes [9] that might lead to significant microstructural distortions.

SEM micrographs of coarse-structured anodes did not reveal any significant changes in the microstructure. No major sintering and agglomeration of nickel particles was observed, and the porosity seemed to be unchanged (Fig. 5).

3.2. Electrochemical testing

3.2.1. Fine-structured anode powder

Electrochemical testing of the cell started with overnight reduction of the anode. After a stable OCV of 0.98 V was reached, a constant load was applied. The results of previous studies [13] show that anode-supported SOFC cells experience a significant increase in performance within the first couple of days. The tested cells, of this current study, were consistent with previous data. Significant increase in performance was observed,

Table 2
A comparison of average fracture strength, standard deviation and Weibull parameter of fine and coarse-structured anode powder subjected to redox cycling

Cycle	σ_{avg} (Mpa)		Standard deviation		Weibull parameter	
	Coarse structure	Fine structure	Coarse structure	Fine structure	Coarse structure	Fine structure
Non-reduced anode	75.5	65.1	2.6	3.8	27	16
Reduced anode	53.0	69	2.5	6.7	18	10
First redox	68.5	98.6	1.5	12.5	46	8
Second redox	63.4	118	8.4	23	7	5
Third redox	58.8	122.4	11.4	5.5	5	22
Fourth redox	51.7	105.3	10.3	9.8	5	10
Fifth redox	51.0	105.3	18.3	15.8	2	6

and after approximately 72 h, the cell performance stabilized. The improvement in performance is believed to be due to the increase of catalytic activity of the anode.

Within minutes following the first redox cycle, the OCV was restored. However, the OCV reached only 0.79 V; which is significantly lower than the value obtained before the redox cycle. One of the reasons for the decrease in OCV is possibly due to micro-crack formation of the electrolyte due to the volumetric anode changes. SEM micrographs, however, did not reveal any electrolyte cracking.

In order to verify the maximum power density, *V–I* curves were performed after each redox cycle. The *V–I* curve performed after the first redox cycle resulted in a maximum power density of 0.67 W cm^{-2} achieved at 0.48 V, which is 40% higher in comparison to 0.48 W cm^{-2} at 0.48 V reached before the first redox cycle (Fig. 6). The cell was then operated at constant current of 1 A cm^{-2} for 30 min. The performance was stable and no decrease in power density was observed during the time of experiment (Fig. 7).

The second redox cycle resulted in highly unstable OCV conditions. The *V–I* curve produced a maximum power density of 0.56 W cm^{-2}, which was lower than the value obtained after the first redox cycle. In addition to these results, the applied load resulted in a gradual decrease in performance. The cell cracked after about 7.5 h following the second redox cycle.

It is believed that the volumetric changes in the nickel particles experienced during redox cycling resulted in micro-crack formation of the YSZ electrolyte layer. Hydrogen cross-over through the electrolyte is the most common reason for low OCV and causes localized LSM cathode reduction. An optical microscopy investigation of the cathode surface at the end of the study revealed significant partial cathode reduction. However, it is not clear if the cathode was partially reduced due to hydrogen leakage through the micro-cracks in the electrolyte layer, or if the reduction was caused by the crack of the cell after the second redox cycle.

Even though the OCV was much lower than the value obtained before redox cycling, the overall power density improved significantly. The mechanism of this performance improvement is still not fully understood. One hypothesis suggests an improvement in electrical contact between the nickel

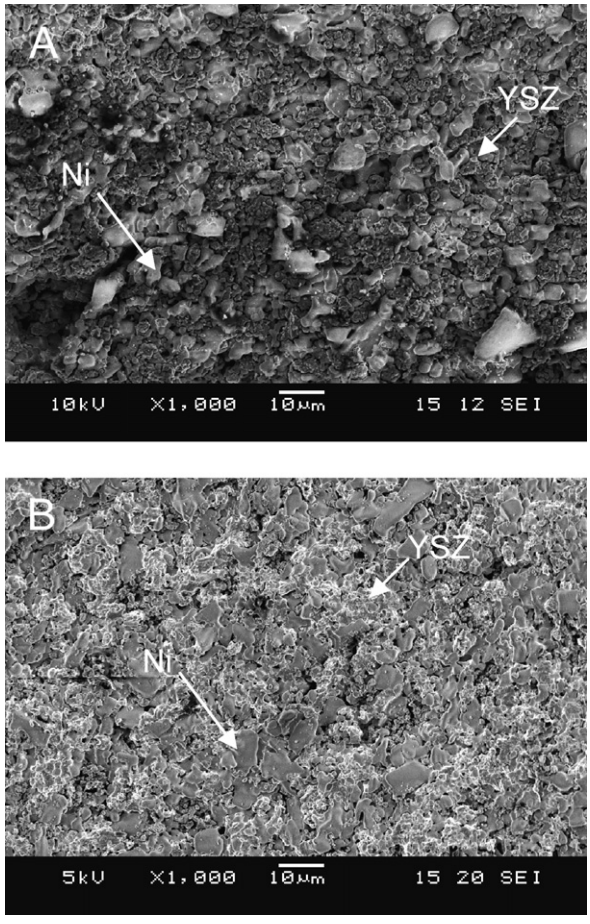

Fig. 5. SEM micrographs of the coarse-structured Ni/8YSZ anodes (A) after reduction and (B) after the third redox cycle.

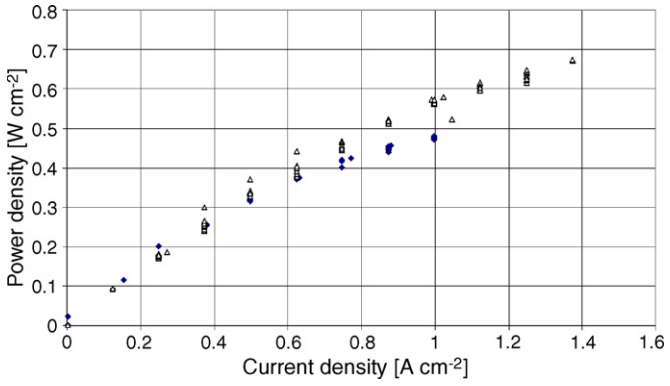

Fig. 6. Power density vs. current density for reduced cell (♦) and cell after the first redox cycle (△)

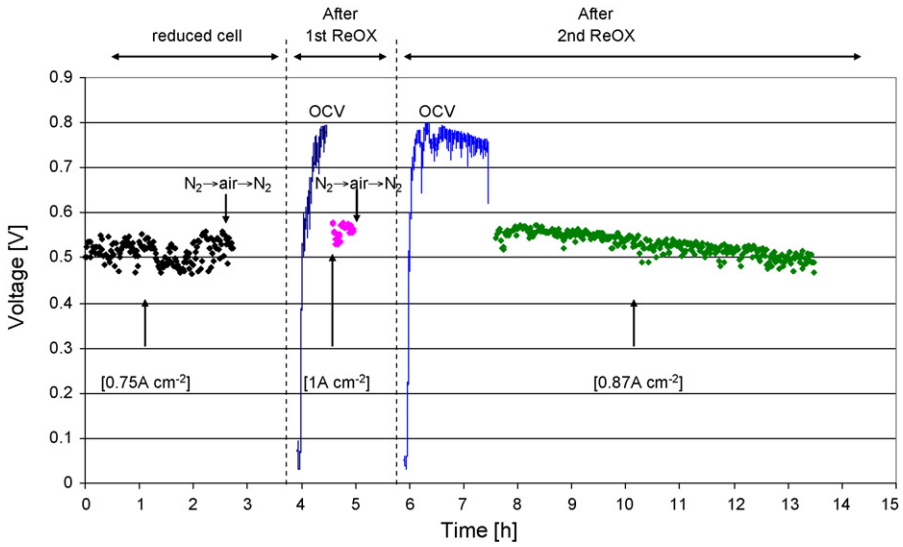

Fig. 7. SOFC performance before and after exposing to redox cycle.

wire and the cermet anode. The theory is supported by several markings produced by the current collector wire at the anode surface (Fig. 8). Such markings show chemical interaction between the nickel wire and the anode. It is believed that the chemical interaction was triggered by the oxidation and reduction of the nickel wire during redox cycling. Due to the volumetric expansion, the wire was pressed against the surface of the cermet anode improving the contact between the nickel wire and the cermet anode.

Similar markings at the anode surface were found only in prior cases of cells that were operated under load conditions for several weeks. Short-term testing has never produced similar results.

It could be also postulated that hydrogen leaking through the micro-cracks in the electrolyte combusted increasing the operating temperature of the cell. As a result, an improvement in performance would be noticed.

3.2.2. *Coarse-structured anode*

The cell fabricated using a coarse-structured anode powder before redox cycling presented very similar results to the fine-structured anodes. However, the cell did not recover after the first redox cycle and further electrochemical testing was impossible.

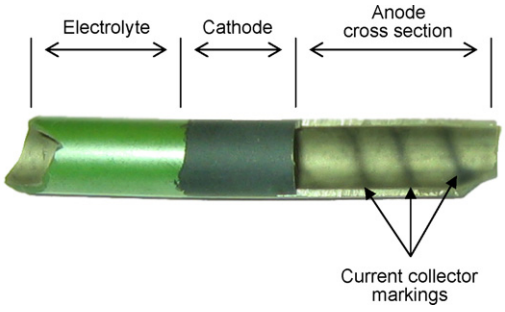

Fig. 8. A photograph of the cell after redox cycling. The cross-section area reveals current collector markings.

4. Conclusions

Redox cycling of Ni/8YSZ supported SOFC introduces significant changes in the mechanical stability of the cell, and surface adhesion between the nickel-based anode and nickel current collector. While the mechanism of the reaction is not fully understood it shows a possibility of electrochemical contact enhancement between the nickel current collector and the cermet anode.

The anode powder processing technologies and the powder morphology, especially particle size, are significant factors in the response of the cell to redox cycling. The anodes fabricated using commercially available fine-structured powder produced an increase in mechanical stability and improvement of electrochemical performance after exposing to redox cycle. The same study based on the anodes fabricated using commercially available coarse-structured powders did not produce similar results; further suggesting the significance of particle size in cell response to redox cycling.

Acknowledgement

This work was supported by NEDO, as part of the Advanced Ceramic Reactor Project.

References

[1] A. Weber, B. Sauer, A.C. Müller, D. Herbstritt, E. Ivers-Tiffée, Solid State Ionics 152–153 (2002) 543–550.
[2] C. Finnerty, G.A. Tompsett, K. Kendall, R.M. Ormerod, J. Power Sources 86 (2000) 459–463.
[3] J. Staniforth, K. Kendal, J. Power Sources 86 (2000) 401–403.
[4] J.B. Wang, J.C. Jang, T.J. Huang, J. Power Sources 122 (2003) 122–131.
[5] G.J. Saunders, K. Kendall, J. Power Sources 106 (2002) 258–263.
[6] J. Liu, S.A. Barnett, Solid State Ionics 158 (2003) 11–16.
[7] N.M. Sammes, R.J. Boersma, G.A. Tompsett, Solid State Ionics 135 (2000) 487–491.

[8] H. Itoh, Y. Heie, T. Yamamoto, M. Mori, T. Watanabe, in: H. Yokokawa, S.C. Singhal (Eds.), The Electrochemical Society Proceedings of the Solid Oxide Fuel Cells VII, Pennington, NJ, PV2001-16, 2001, p. 750.
[9] D. Waldbillig, A. Wood And, D.G. Ivey, Solid State Ionics 176 (9–10) (2005) 847–859.
[10] R. Peraldi, D. Monceau, B. Pieraggi, Oxid. Met. 58 (October (3–4)) (2002) 275–295.
[11] W. Suwanwatana, S. Yarlagadda, J.W. Gillespie, J. Mater. Sci. 38 (3) (2003) 565–573.
[12] R. Karmhag, G.A. Niklasson, M. Nygren, J. Appl. Phys. 85 (2) (1999) 1186–1191.
[13] J. Pusz, A. Mohammadi, N.M. Sammes, J. Fuel Cell Sci. Technol., 2006, in press.